RETRACTED: Application of Nanopharmaceutics for Flibanserin Brain Delivery Augmentation Via the Nasal Route

Osama A. A. Ahmed [1,2], **Usama A. Fahmy** [1,*], **Shaimaa M. Badr-Eldin** [1,3],
Hibah M. Aldawsari [1], **Zuhier A. Awan** [4], **Hani Z. Asfour** [5], **Ahmed K. Kammoun** [6],
Giuseppe Caruso [7], **Filippo Caraci** [7,8], **Anas Alfarsi** [1], **Raniyah A. Al-Ghamdi** [9],
Rawan A. Al-Ghamdi [10] and **Nabil A. Alhakamy** [1,2,11]

[1]   Department of Pharmaceutics, Faculty of Pharmacy, King Abdulaziz University, Jeddah 21589, Saudi Arabia;
    oaahmed@kau.edu.sa (O.A.A.); smbali@kau.edu.sa (S.M.B.-E.); haldosari@kau.edu.sa (H.M.A.);
    mr_alfarsi8@hotmail.com (A.A.); nalhakamy@kau.edu.sa (N.A.A.)
[2]   Advanced Drug Delivery Research Group, Faculty of Pharmacy, King Abdulaziz University,
    Jeddah 21589, Saudi Arabia
[3]   Department of Pharmaceutics and Industrial Pharmacy, Faculty of Pharmacy, Cairo University,
    Cairo 11562, Egypt
[4]   Department of Clinical Biochemistry, Faculty of Medicine, King Abdulaziz University,
    Jeddah 21589, Saudi Arabia; zawan@kau.edu.sa
[5]   Department of Medical Microbiology and Parasitology, Faculty of Medicine, King Abdulaziz University,
    Jeddah 21589, Saudi Arabia; hasfour@kau.edu.sa
[6]   Department of Pharmaceutical Chemistry, Faculty of Pharmacy, King Abdulaziz University,
    Jeddah 21589, Saudi Arabia; akammoun@kau.edu.sa
[7]   Oasi Research Institute—IRCCS, Via Conte Ruggero, 73, 94018 Troina (EN), Italy; gcaruso@oasi.en.it (G.C.);
    carafil@hotmail.com (F.C.)
[8]   Department of Drug Sciences, University of Catania, 95125 Catania, Italy
[9]   Ibn Sina National College for Medical Studies, Clinical Pharmacy Department, Jeddah 22421, Saudi Arabia;
    Ranoabg@hotmail.com
[10]   Ibn Sina National College for Medical Studies, Jeddah 22421, Saudi Arabia; rawanaasg3@gmail.com
[11]   Center of Excellence for Drug Research and Pharmaceutical Industries, King Abdulaziz University,
    Jeddah 21589, Saudi Arabia
*   Correspondence: uahmedkauedu.sa@kau.edu.sa; Tel.: +966-599120686

Abstract: Flibanserin (FLB) is a nonhormonal medicine approved by the Food and Drug Administration (FDA) to treat the hypoactive sexual appetite disorder in females. However, the peroral administration of the medicine is greatly affected by its poor bioavailability as a result of its extensive first-pass effect and poor solubility. Aiming at circumventing these drawbacks, this work involves the formulation of optimized FLB transfersome (TRF) loaded intranasal hydrogel. Box–Behnken design was utilized for the improvement of FLB TRFs with decreased size. The FLB-to-phospholipid molar ratio, the edge activator hydrophilic lipophilic balance, and the pH of the hydration medium all exhibited significant effects on the TRF size. The optimized/developed TRFs were unilamellar in shape. Hydroxypropyl methyl cellulose based hydrogel filled with the optimized FLB TRFs exhibited an improved ex vivo permeation when compared with the control FLB-loaded hydrogel. In addition, the optimized TRF-loaded hydrogel exhibited higher bioavailability and enhanced brain delivery relative to the control hydrogel following intranasal administration in Wistar rats. The results foreshadow the possible potential application of the proposed intranasal optimized FLB-TRF-loaded hydrogel to increase the bioavailability and nose-to-brain delivery of the drug.

Keywords: flibanserin; transfersomes; hydrogel; ex vivo permeation; in vivo pharmacokinetics

1. Introduction

Flibanserin (FLB) is a recently FDA-approved nonhormonal drug for the treatment of women with hypoactive sexual appetite disorder. FLB acts via decreasing the level of serotonin and increasing the levels of dopamine and norepinephrine for maintaining healthy sexual response [1]. FLB-treated women have demonstrated significant improvements in both the number of satisfying sexual events and the female sexual function index desire domain score compared placebo-treated ones. These findings proved the ability of the drug to enhance the women's sexual desire. In addition, administration of FLB was linked with a significant reduction in the distress related with either sexual dysfunction or low sexual desire [2–5]. However, the major challenge for oral administration of FLB is the reduced bioavailability (~33%) that might be caused by the drug's low solubility and its exposure to hepatic first-pass metabolism [6,7].

Recently, intranasal drug administration has gained increasing interest. The nasal pathway is a noninvasive route for active pharmaceutical ingredient (API) administration with the aim of local, systemic, or central nervous system (CNS) action. The nasal cavity represents an ideal absorption surface for drug delivery due to the high vascularity of this area, in addition to the leaky epithelium that results from the low tightness of the intercellular nasal mucosal junctional complex. Furthermore, direct absorption of the molecules from the nasal cavity via the trigeminal and olfactory pathways provides direct entry into the brain and results in a favorable pharmacokinetic/pharmacodynamic profile for centrally acting drugs. Thus, the nasal route could offer an encouraging unconventional approach to enteral and systemic drug administration of CNS-targeting drugs [8,9].

Transfersomes (TRFs), also called deformable or elastic liposomes, are flexible vesicular systems that involve a phospholipid (PL) and an edge activator. They are considered as a modified generation of liposomes and were firstly modified by Cevc and Blume [10] by adding edge activators. The edge activators are usually a single-chain surfactant which enhances the squeezing and penetration of the vesicles through the mucosal barrier through destabilization of the lipid bilayers. The commonly used edge activators include sodium deoxycholate, sodium cholate, Tween, and Span [11–13]. Intranasal administration of TRFs has been previously reported to enhance bioavailability of several drugs [14–16]. Moreover, TRFs have been effectively applied for enhancing brain distribution of centrally acting medicines [17–19].

Hydrogel-loaded nanoformulated drugs have drawn significant attention as promising nanoparticulate drug delivery systems that combine both hydrogel system properties (e.g., hydrophilicity and high water absorption affinity) and nanoparticulate properties (e.g., ultrasmall size) [20–27], can achieve high drug loading without chemical reactions, and are able to release integrated agents at the target site in a controlled behavior. A wide range of natural, naturally derived and synthetic hydrogels can be used for hydrogel-loaded nanoformulated drug preparation [26–28]. Hydrogels can be prepared from naturally derived protein or polysaccharide polymers [29]. The synthetic hydrogels have drawn great attention in the biomedical field [30,31]. The synthetic hydrogels are obtained through chemical and physical methods. Among the synthetic hydrogels, poly(2-isopropenyl-2-oxazoline) (PiPOx) is a biocompatible polymer synthesized using a simple protocol [30]. In addition, poly(vinyl alcohol) (PVA) and PVA/poly(ethylene glycol) (PEG) hybrid hydrogels were synthesized that showed improved mechanical strength when compared with PVA hydrogel [32].

Among natural and naturally derived hydrogels, the most frequently used are polysaccharides. Materials with polysaccharides can be divided into two groups, namely polyelectrolytes and non-polyelectrolytes. Additionally, polyelectrolytes may be classified according to their intrinsic charges, including cationic (chitosan), anionic (alginate, heparin, pectin, hyaluronic acid), and neutral (pullulan, dextran). Due to their desirable mucoadhesive properties, cellulose derivatives can significantly extend the residence time of drugs in the nasal cavity [33]. Furthermore, due to their high

viscosity following hydration in the nasal cavity, celluloses can sustain the release of drugs. For these reasons, the use of cellulose as an absorption enhancer can lead to improved intranasal absorption and increased bioavailability [34]. Reports show that celluloses increase the intranasal bioavailability of both small hydrophobic and hydrophilic macromolecular drugs [35]. Hydroxypropyl methyl cellulose (HPMC) is a popular matrix material in controlled drug delivery systems, and HPMC matrices show a sustained release pattern by two mechanisms, i.e., diffusion and erosion of the gel layer [36]. The viscosity of the polymer affects the diffusion pathway. HPMC can be employed as a matrix for controlling the release of both hydrophilic and hydrophobic drugs [37]. HPMC-based gels showed good surface morphology with high drug loading efficiency. The viscosities of the preparations were found to be within a suitable range for nasal administration.

Therefore, the main aim of this study was to acquire an optimized FLB-TRF-loaded HPMC-based hydrogel for an improved drug delivery to the brain via intranasal administration. Box–Behnken design was utilized for FLB TRF optimization. The effects of FLB-to-PL molar ratio, edge activator hydrophilic lipophilic balance (HLB), and pH of hydration medium on vesicle size were studied. The optimized TRFs with minimized vesicle size were prepared and fused into hydroxypropyl methyl cellulose based hydrogel. The prepared hydrogel was assessed for shape characteristics and ex vivo permeation. In addition, in vivo performance was evaluated after intranasal administration in Wistar rats.

2. Materials and Methods

2.1. Materials

Flibanserin (FLB) was purchased from Qingdao Sigma Chemical Co., Ltd. (Qingdao, China); Phospholipon 90G (phosphatidyl choline from soy, at least 90% purity) was purchased from Lipoid GmbH (Frigenstr, Ludwigshafen, Germany); Span 65, Span 80, methanol, and chloroform were purchased from Sigma-Aldrich Co. (St. Louis, MO, USA).

2.2. FLB TRF Preparation

FLB TRFs were prepared by the hydration of the formed lipid film as previously described [38]. Briefly, specified amounts of FLB, PL, and edge activator (surfactant) were dissolved in methanol/chloroform mixture (1:1, *v/v*) and subjected to water bath sonication for 5 min. The amounts of FLB, PL, and surfactant were specified according to Table 1. Span 65 and span 80 were used in different ratios to achieve the required HLB value of the edge activator indicated in the design (Table 1). The solution was then evaporated using a rotary evaporator at 45 °C. The formed film was kept in a vacuum oven overnight for complete removal of solvent residuals. Subsequently, the dried thin film was hydrated with 20 mL of buffer solution, according to the specified pH, for 3 h at 25 °C with gentle shaking.

2.3. Box–Behnken Design for FLB TRF Preparations

According to the previous screening results conducted in our laboratory, the optimization of FLB TRFs was carried out to achieve minimal size. FLB:PL molar ratio (X_1), HLB (X_2), and pH of hydration medium (X_3) were the investigated factors, while vesicle size (Y_1) was the studied response. The X_1 ratios studied were 1:1, 1:3, and 1:5; X_2 values were 2, 4, and 6; and X_3 values were 5, 7, and 9. All other processing and formulation variables, including drug amount (10% *w/w*), were kept constant throughout the study. The experimental design using Design-Expert software (version 12; Stat-Ease, Inc., Minneapolis, MN, USA) yielded 17 formulations. The actual values of the independent variables of these runs and the observed responses are presented in Table 1. The measured responses were statistically analyzed by the analysis of variance (ANOVA) test. The polynomial equations representing the best fitting model for each variable was generated. Three-dimensional surface plots were plotted to illustrate the impact of the variables and interaction between them at $p < 0.05$. Afterwards, a numerical method following the desirability approach was utilized to

predict the optimized FLB TRFs. The predicted formulation was then prepared and further evaluated. The measured responses were compared to the predicted ones, and the residual error was calculated to ensure the success of the optimization process.

Table 1. Experimental runs and the observed vesicle size of flibanserin (FLB) transfersomes (TRFs) according to Box–Behnken design.

Experimental Run Number	Independent Variables			Vesicle Size (nm) ± SD
	FLB:PL Molar Ratio *	Surfactant HLB	Hydration Medium pH	
T1	3.00	4.00	7.00	121 ± 2.81
T2	3.00	6.00	9.00	127 ± 1.78
T3	3.00	2.00	9.00	128 ± 3.11
T4	5.00	4.00	9.00	166 ± 1.12
T5	1.00	4.00	5.00	111 ± 1.65
T6	3.00	4.00	7.00	122 ± 1.27
T7	5.00	6.00	7.00	174 ± 2.18
T8	3.00	4.00	7.00	123 ± 2.09
T9	1.00	6.00	7.00	96 ± 1.03
T10	3.00	6.00	5.00	177 ± 1.99
T11	1.00	2.00	7.00	89 ± 0.99
T12	5.00	2.00	7.00	155 ± 1.45
T13	1.00	4.00	9.00	88 ± 0.86
T14	3.00	2.00	5.00	144 ± 2.56
T15	5.00	4.00	5.00	175 ± 2.43
T16	3.00	4.00	7.00	123 ± 1.49
T17	3.00	4.00	7.00	125 ± 1.66

Notes: * FLB:PL molar ratio were coded 1, 3, and 5 for 1:1, 1:3, and 1:5 FLB:PL ratios, respectively. Abbreviations: FLB, flibanserin; PL, phospholipid; SD, standard deviation.

2.4. Vesicle Size Determination

The vesicle size of freshly prepared FLB TRF was measured using a Zetasizer Nano ZSP (Malvern Panalytical Ltd. Malvern, UK). The result is expressed as the mean of five determinations.

2.5. Characterization of Optimized FLB TRFs

For investigation of vesicle size, polydispersity index (PDI), and zeta potential of the optimized FLB TRFs, the same method mentioned in Section 2.4 using a Malvern size analyzer was employed. In addition, optimized FLB TRFs were subjected to transmission electron microscopy (TEM). A sample was placed on a copper grid and stained using phosphotungstic acid. After removing excess stain, the stained sample was dried and studied using a JEOL-JEM-1011 transmission electron microscope (JEOL, Tokyo, Japan).

2.6. Preparation of Optimized FLB-TRF-Loaded Hydrogel

Optimized FLB TRFs were incorporated into hydroxypropyl methyl cellulose (HPMC) based hydrogel. Briefly, specified amount of HPMC (0.1 g) was dispersed in distilled (10 mL) water to make a 1% *w/v* concentration. The gel was kept in the refrigerator overnight and then FLB TRFs were added with continuous stirring to obtain a drug concentration of 10 mg/g. Control hydrogels incorporating raw drug (10 mg/g gel) were prepared under the same conditions for comparison.

2.7. Optimized FLB TRF Gel Ex Vivo Permeation Study

Freshly excised goat nasal mucosa was utilized for ex vivo permeation studies. Mucosa were equilibrated in simulated nasal fluid (SNF) with pH 6.8 for 15 min. SNF was composed of sodium chloride (0.877%), calcium chloride (0.058% *w/v*), and potassium chloride (0.298% *w/v*) dissolved in deionized water [39]. Mucosa and gel samples were mounted between the two chambers and the donor

chamber [40]. The area of the chamber of the utilized Franz automated diffusion cell (MicroettePlus; Hanson Research, Chatsworth, CA, USA) was 1.76 cm^2. Gels loaded with optimized FLB TRF or raw FLB (0.1 g each 10 mg FLB/g gel) were utilized in this study. Seven milliliters of simulated nasal fluid (SNF) with pH 6.8 was used in the receiver chamber as the diffusion medium that was kept at 35 ± 0.5 °C with the agitation rate set at 400 rpm. At specified time intervals, 1.5 mL aliquots were withdrawn and replaced with fresh SNF.

2.8. In Vivo Pharmacokinetic Assessment

The pharmacokinetic performance of the FLB-TRF-loaded hydrogel was investigated in Wistar rats, weighing 200–250 g each, and compared to control raw-FLB-loaded gel. The study protocol was approved by the Research Ethics Committee, Faculty of Pharmacy, King Abdulaziz University, Kingdom of Saudi Arabia, under approval number (PH-124-41). The committee ensures that animal use complies with the European Union Directive 2010/63/EU and the DHEW Publication NIH 80-23 Guiding Principles. The study included two animal groups (I and II), with all animals receiving FLB dose of 10 mg/kg intranasally. Group I received raw FLB gel, and group II received FLB-TRF-loaded hydrogel. Collection of blood samples was performed at specified time intervals. Six rats from each group were sacrificed at each time interval, and the whole brain was washed with saline after removal and then weighed. Brain tissues were homogenized with phosphate buffer (pH 7.4) at 5000 rpm for 3 min. Plasma and homogenized brain samples were stored at −80 °C prior to analysis [41].

A volume of 200 μL of plasma sample, along with 200 μL of the brain homogenate, was transferred to a screw-capped test tube, mixed with 50 μL internal standard solution (valsartan, 625 ng/μL) and 1 mL acetonitrile, vortexed for 1 min, and then centrifuged at 5300 rpm for 8 min. An aliquot of the clear supernatant was transferred to a total recovery autosampler vial, and a volume of 7 μL was injected for LC-MS/MS-DAD analysis. The MS system was connected to an Agilent 1200 HPLC system equipped with an autosampler, a quaternary pump, and a column compartment (Palo Alto, CA, USA). The system was equipped with ChemStation software (Rev. B.01.03 SR2 (204)). The IT–MS was controlled using 6300 series trap control version 6.2 Build No. 62.24 (Bruker Daltonik GmbH), and the general MS adjustments were as follows: capillary voltage, 4200 V; nebulizer, 37 psi; drying gas, 12 L/min; desolvation temperature, 330 °C; ion charge control (ICC) smart target, 200,000; and max accumulation time, 200 ms. The MS scan range was 50–550 m/z. For quantitative monitoring, single positive molar ion mode was applied at programed time segment, 0–4.0 min, m/z 391.2 [M+H]+ FLB; 4.0–10 min, m/z 436.3 [M+H]+ internal standard. Isocratic elution was conducted at a flow rate of 0.5 mL/min with a mobile system composed of 52% acetonitrile and 48% water containing 0.1% formic acid. FLB content in the assayed samples was quantified with reference to a calibration curve (range of 1–1000 ng/mL). The calibration curves for FLB were assessed using free-drug-plasma and free drug brain homogenate matrixes as a calibration matrix. The stock solutions of FLB and valsartan (InSt) were prepared separately by dissolving 10 mg of each in methanol to obtain a concentration of 0.1 mg/mL. A series of calibrator working solutions of FLB were prepared from its stock solutions by applying a serial dilution technique and using methanol as the diluting solvent. The calibration solutions were prepared by spiking the plasma-free drug with FLB solutions to give a concentration spanning the range of 1.0 to 1000.0 ng/mL of FLB and a fixed InSt concentration of 25 μg/mL. The calibrated solutions were extracted and analyzed by the developed method. The peak area ratios of FLB-to-InSt were found to be linear in the concentration range of 1.0 to 1000 ng/mL of FLB. Pharmacokinetic parameters including the maximum plasma concentration (C_{max}), time to maximum plasma concentration (T_{max}), and area under the plasma concentration–time curve ($AUC_{0-\infty}$) were calculated using Kinetica software (Version 4; Thermo Fisher Scientific, Waltham, MA, USA). The parameters were analyzed for significance using SPSS software (Version 16; SPSS Inc., Chicago, IL, USA). Unpaired Student's *t*-test was performed on C_{max} and $AUC_{0-\infty}$, while the nonparametric Mann–Whitney test was utilized for analysis of T_{max}; a level of significance of $p < 0.05$ was set for all investigated pharmacokinetic parameters. For histopathological evaluation, 12 rats were divided into four groups: untreated rats (gp1), rats

treated with plain in situ gel without drug (gp2), rats that received FLB drug in the in situ gel (gp3), and rats treated with FLB-Nanostructured lipid carriers (FLB-NLCs, gp4). The same dosing procedure as previously described in the pharmacokinetics study was used. After 8 h, histopathologic analysis was conducted according to the method of Young [42]. In brief, the head was removed, and the brain and jaw were removed from the head along with any other listed tissues. The nasal cavity was initially fixed in a solution of 10% formalin and then decalcified in a solution of 10% EDTA. The tissue was then placed in 70% ethanol before being embedded in paraffin, sectioned, and stained with hematoxylin and eosin.

2.9. Statistical Analysis

For the in vivo data, the software selected to perform the statistical analysis was GraphPad Prism (San Diego, CA, USA). One-way or two-way analysis of variance (ANOVA), followed by Tukey's post hoc test, was used for multiple comparisons. Only values of $p < 0.05$ were considered statistically significant. Each set of experiments was performed at least in triplicate and is reported as means ± SD. For the in vitro Box–Behnken design data, the effects of factors on the response (vesicle size) were statistically analyzed by ANOVA using the Design-Expert software.

3. Results

3.1. Polynomial Model Selection and Diagnostic Analysis

The observed vesicle size of the prepared TRFs best fitted to the quadratic model based on its highest correlation coefficient (R^2) is shown Table 2. There was a satisfactory agreement between the predicted and adjusted R^2, indicating that the selected model was valid for analyzing the data. Moreover, an adequate precision value of greater than 4 indicates an adequate signal-to-noise ratio, implying the suitability of the quadratic model to navigate the design space. Diagnostic plots were generated to ensure the goodness of fit of the chosen model. Figure 1A, illustrating the residual vs. run plots, shows randomly scattered points, indicating that there is no lurking variable interfering with the vesicle size. Furthermore, the high linearity illustrated in the predicted versus actual values plot (Figure 1B) indicates that the observed vesicle size was analogous to the predicted one.
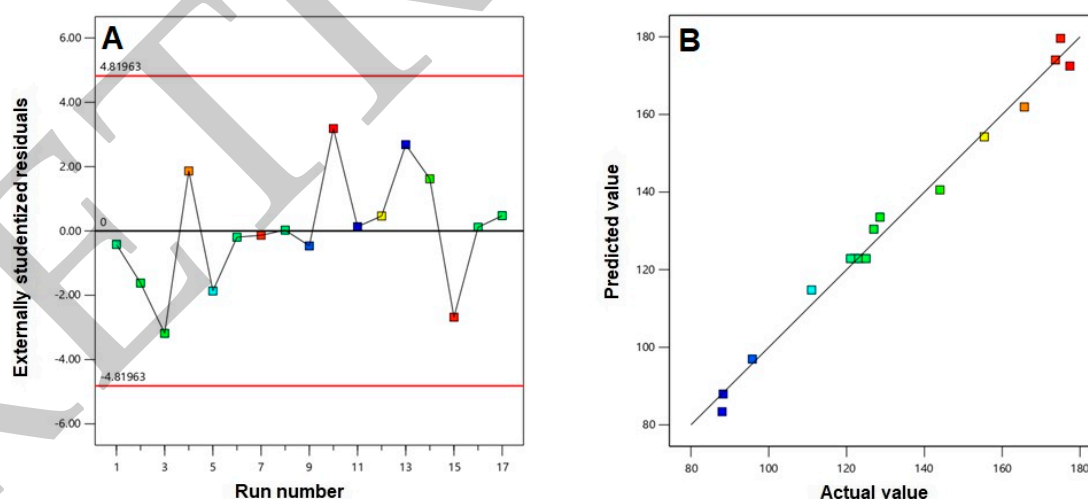
Figure 1. Diagnostic plots for flibanserin (FLB) transfersome (TRF) vesicle size: (**A**) externally studentized residuals vs. run number plot; (**B**) predicted vs. actual values plot.

Table 2. Statistical analysis of the measured FLB TRF vesicle size, the composition of the optimized formulation, and its predicted and observed responses.

Factor	Optimum Level		Low Level			High Level
X_1: FLB:PL molar ratio	1:1.2		1:1			1:5
X_2: Surfactant HLB	2.3		2			6
X_3: Hydration medium pH	7.2		5			9
Response	Predicted		Actual			Residual error %
Vesicle size (nm)	87.89		89.71			2.07%
Statistical analysis output of TRF vesicle size (Quadratic model)	R^2		Adjusted R^2		Predicted R^2	Adequate precision
	0.9885		0.9738		0.8262	26.6354
	p-value	X_1	X_2	X_3	$X_{2 \times 3}$	$X_2{}^2$	$X_3{}^2$
		0.0001	0.0035	0.0002	0.0075	0.0148	0.0005

Abbreviations: FLB, flibanserin; PL, phospholipid.

3.2. Statistical Analysis for the Effect of Variables on Vesicle Size (Y)

The size of vesicles is a critical parameter that exhibits a significant impact on the drugs' permeation via the biological membranes. FLB TRF showed size in the nanoscale range with mean size ranging from 88 ± 0.86 to 175 ± 2.43 nm (Table 1). The relatively small standard deviation could indicate homogeneity of the TRF dispersions. The equation representing the selected sequential model was generated in terms of coded factors as follows:

$$Y_1 = 122.88 + 35.84\,X_1 + 7.20\,X_2 - 12.70\,X_3 + 2.70\,X_{1 \times 2} + 3.42\,X_1 X_3 - 8.75\,X_2 X_3 - 1.95\,X_1{}^2 + 7.37\,X_2{}^2 + 14.00\,X_3{}^2 \tag{1}$$

The statistical analysis revealed that all the linear terms corresponding to the three investigated variables have a significant negative effect on FLB TRF size ($p < 0.05$). The quadratic terms corresponding to the surfactant HLB ($X_2{}^2$) and hydration medium pH ($X_3{}^2$), in addition to the interaction term $X_2 X_3$ corresponding to the interaction between the two aforementioned variables, were also found to be significant at the same significance level. Figure 2 illustrates the contour plots for the investigated variable effects on vesicle size.

3.3. FLB TRF Optimization

The formation of the optimized FLB TRFs was accomplished using a numerical optimization technique with a minimized vesicular size. The optimized formulation was prepared at factor levels of 1:1.12 FLB:PL molar ratio, HLB value of 2.3, and hydration medium pH of 7.2. The observed and predicted values of the optimized FLB TRF formulation were in good agreement (with low error percentage), confirming the reliability of the optimization process (Table 2).

3.4. Characterization of the Optimized FLB TRFs

The PDI of the optimized formulation was found to be 0.201 ± 0.012, while the zeta potential was equal to 8.12 ± 1.54 mV. TEM has been applied for assessing of the shape and lamellarity of the optimized FLB TRF at 25,000× magnification. As illustrated in Figure 3, the TRF showed vesicles with spherical shape. No aggregation was observed. In addition, the recorded size was within an acceptable agreement with that recorded using the dynamic light scattering technique of the particle size analyzer.
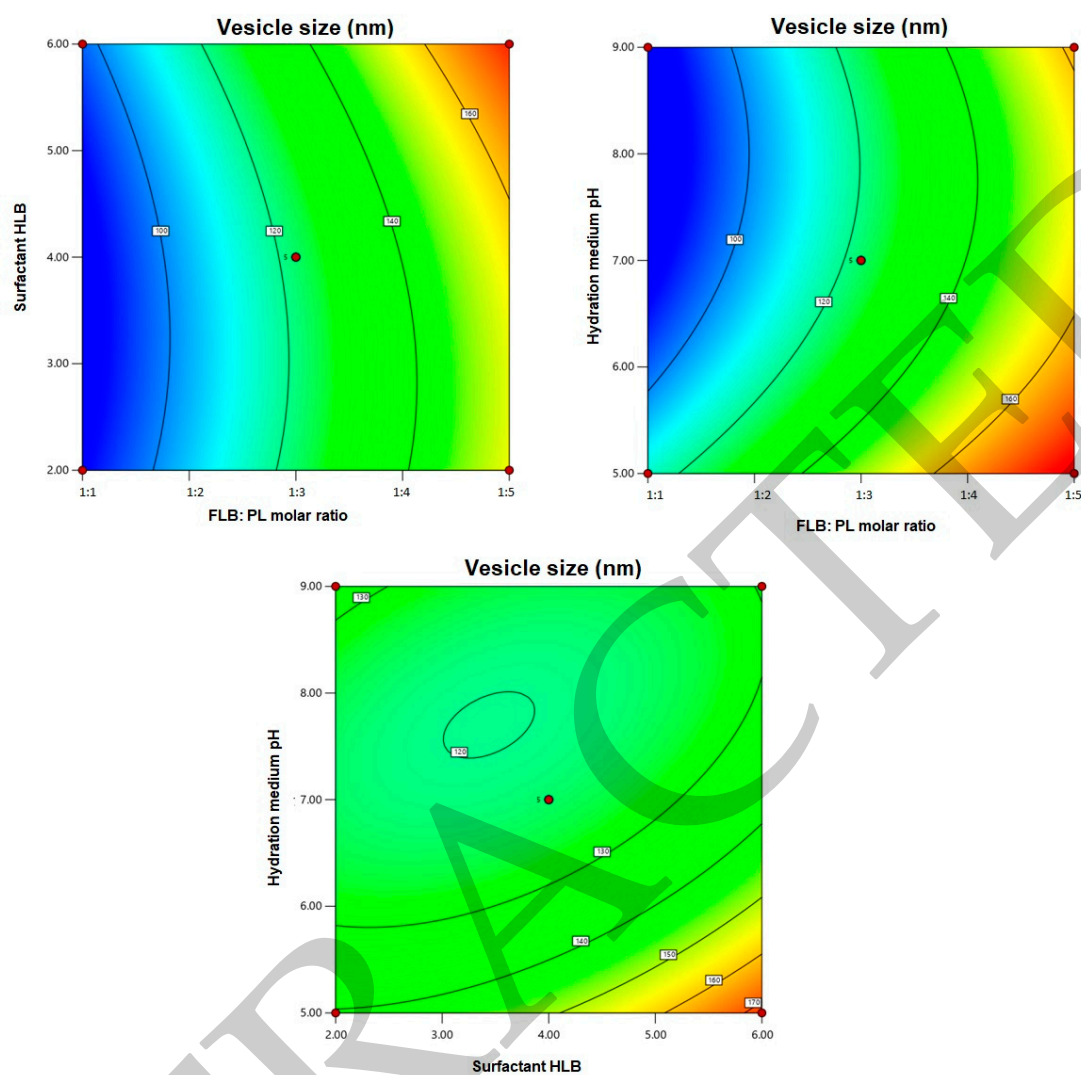
Figure 2. Contour plot for the effects of FLB-to-phospholipid (PL) molar ratio (X_1), surfactant hydrophilic lipophilic balance (HLB) (X_2), and hydration medium pH (X_3) on the vesicle size of FLB TRF.
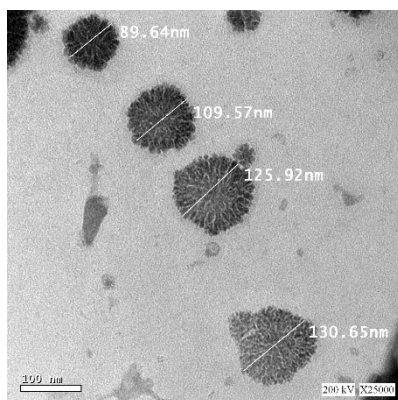

Figure 3. Transmission electron microscope images of optimized FLB TRFs at 25,000× magnification.

3.5. Optimized FLB TRF Gel Ex Vivo Permeation

Ex vivo permeation through goat nasal mucosa was carried out to give an insight into the in vivo performance of the optimized FLB-TRF-loaded hydrogel. Figure 4 illustrates the mean cumulative percent FLB permeated from the TRF-loaded hydrogel (test) compared to FLB-loaded hydrogel (control). The optimized FLB TRF hydrogel shows a significant increase in cumulative percent FLB permeated when compared to raw FLB gel ($p < 0.05$), with almost complete drug permeation after 4 h. The maximum amount of drug permeated within 4 h from optimized FLB TRF hydrogel was approximately 1.97-fold greater than that from raw FLB hydrogel.
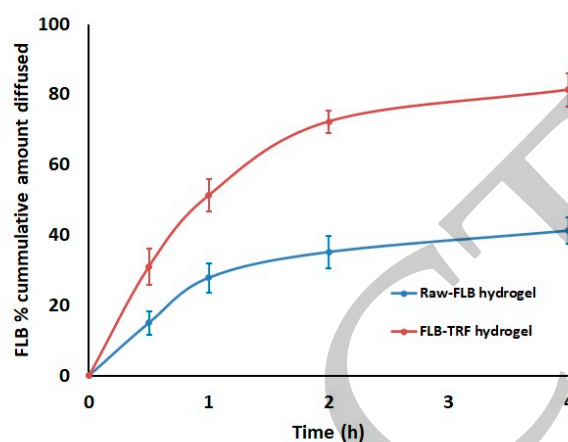
Figure 4. Ex vivo permeation profile of optimized FLB-TRF-loaded intranasal hydrogel compared to raw FLB hydrogel in simulated nasal fluid, pH 6.5, at 35 °C (results presented as mean ± SD, *n* = 3).

3.6. In Vivo Pharmacokinetics

The calibration curves of the concentrations of FLB spiked in plasma and brain homogenate show linear relationships with correlation coefficients of 0.9992 and 0.9984, respectively. The assay shows an adequate precision, with relative standard deviations (RSDs) of 8.1–10.9% and 10.1–12.9% for the intraday assay and the interday assay, respectively. The mean extraction recoveries were 94.8% ± 5.4% and 92.6% ± 7.6% for FLB-spiked plasma and brain samples, respectively. Mean FLB concentrations in plasma and brain following intranasal administration of optimized FLB-TRF-loaded hydrogels, compared to the control FLB-loaded hydrogels, are graphically represented in Figure 5. The computed pharmacokinetic parameters are compiled in Table 3.

Table 3. Pharmacokinetic parameters following intranasal administration of optimized FLB TRF hydrogel compared to raw FLB control hydrogel.

Pharmacokinetic Parameter	Plasma Data		Brain Data	
	Raw FLB Hydrogel	**FLB TRF Hydrogel**	**Raw FLB Hydrogel**	**FLB TRF Hydrogel**
Cmax (ng/mL, plasma) (ng/g, brain)	122.89 ± 4.01	406.81 ± 76.15 [#]	9.70 ± 1.32	20.81 ± 2.30 [#]
AUC$_{0-\infty}$ (ng.hr/mL, plasma) (ng.hr/ng, brain)	296.87 ± 15.18	1188.13 ± 287.16 [#]	85.52 ± 4.34	148.82 ± 12.4 [#]
Tmax (h)	1.0	0.5	4.0	4.0
Relative bioavailability	—–	400.22%	—–	174.02%

Abbreviations: FLB, flibanserin. *n* = 6. [#] Significant at $p < 0.05$, unpaired *t*-test (two-tailed) with Welch's correction compared to raw FLB gel.
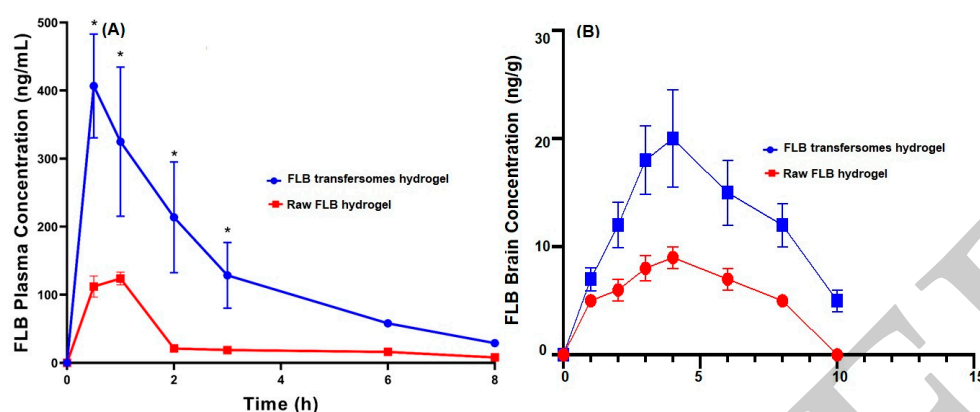
Figure 5. Mean (**A**) plasma concentrations and (**B**) brain concentrations of FLB in rats, plotted against time, after nasal administration of FLB-TRF-loaded intranasal hydrogel compared to control raw FLB hydrogel at a dose of 10 mg/kg. Results presented as mean ± SD, $n = 6$. * Significant at $p < 0.05$, Sidak's multiple comparisons test

From the results of the histopathological evaluation to follow the impact of FLB TRFs on the nasal tissues (Figure 6A–D), no pathological signs of epithelial damage, hyperplasia, edema, or inflammatory infiltration can be see for the four investigated groups.

(**A**)

(**B**)

(**C**)

(**D**)
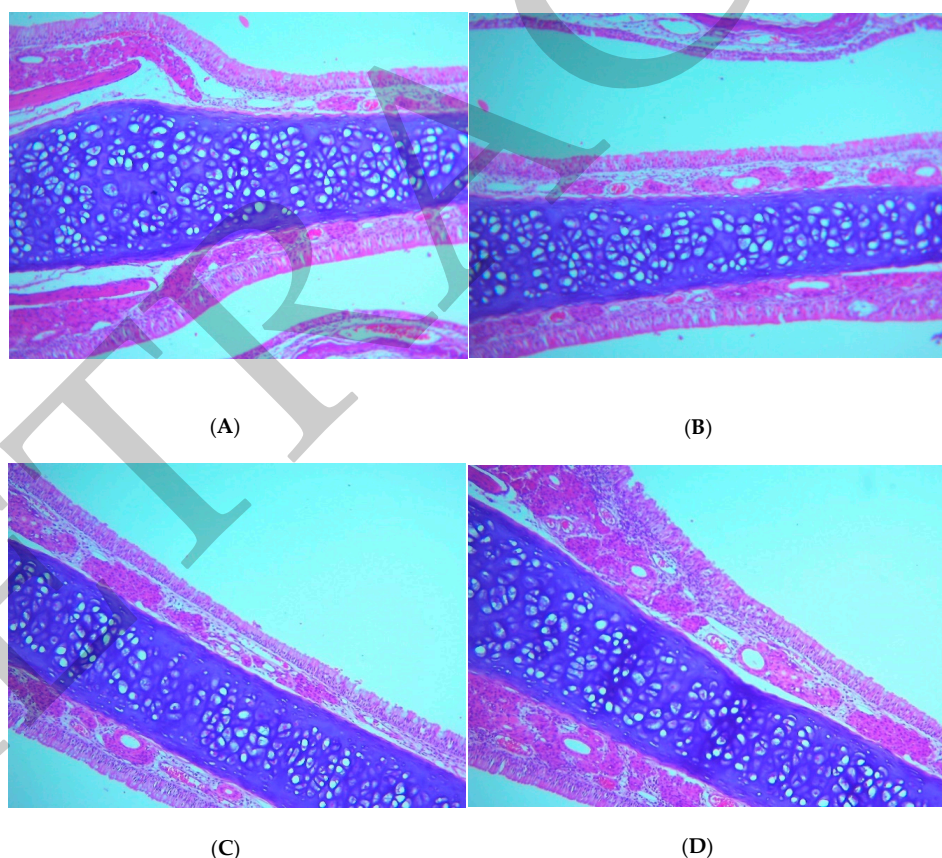
Figure 6. Histopathological results for (**A**) untreated rats (gp1), (**B**) rats treated with plain hydrogel (gp2), (**C**) rats treated with raw FLB loaded in hydrogel (gp3), and (**D**) rats treated with optimized FLB-TRF hydrogel (gp4), showing normal nasal wall with normal intact epithelial lining, average submucosa with average blood vessels, average submucosal cellularity, and average nasal cartilage (H&E, 200× magnification), all of which indicate no increase in submucosal cellularity or tissue abnormality.

4. Discussion

The nanoscale size observed could contribute to enhancing the drug permeation via the nasal mucosa and facilitating passing through the blood–brain barrier. Analysis of variance (ANOVA) for the vesicle size affirmed that the quadratic model was significant ($p < 0.0001$). The positive sign of the coefficients of the linear terms X_1 and X_2 indicates that the vesicle size increases significantly with increasing drug:PL molar ratio and/or surfactant HLB. Contrarily, the negative sign of the linear term X_3 indicates that the vesicle size decreases significantly with increasing hydration medium pH.

The increase of size with increasing drug:PL molar ratio could be credited to increasing the PL content of the vesicles. Similar results were reported for other vesicular systems. Dubey et al. [43] demonstrated increased vesicle size of ethosomes with increasing PL content. In another study, Ahmed and Badr-Eldin [44] reported an increase in avanafil invasome size with increasing PL content of the vesicles. Regarding the HLB of the surfactant, it was observed that a significant reduction of the vesicle size occurs as the HLB is decreased. This observation could be explained on the basis of the increased hydrophobicity of the surfactant with reduced HLB values. Increased surfactant hydrophobicity could lead to reduction of surface energy and low water uptake into the vesicle core, resulting in reduction of the vesicle size [38,45–47]. The boosted FLB permeation from optimized FLB TRF gel could be attributed to the synergistic advantages of TRFs and the nanosized system. The flexible and deformable structure of the TRF could impart the potential to pass easily through the mucosal barriers. Furthermore, the existence of surfactants which act as edge activators could contribute to the permeation-enhancing ability of TRF by disrupting the lipid bilayer of the membrane [46]. In addition, the nanoscale size of the vesicles results in a great surface area, thus increased contact area with the mucosal epithelium and successively improving the chance of drug permeation [38]. Nanovesicles have been reported to have the potential to enhance drug absorption through the nasal membrane barrier and to demonstrate a high efficacy in enhancing drug bioavailability [40]. However, mucociliary clearance can help to reduce the contact time of drug-loaded nanovesicles on the mucosal surface inside the nose. Thus, the application of hydrogel-specific properties is now considered to be a useful platform for the preparation of stabilized and smart nanoscopic vehicles for drug delivery purposes. In addition, the incorporation of transferosomes into the hydrogel network can offer remote-controlled applications and also improve characteristics such as mechanical strength [25,42,48,49]. The observed higher extent of absorption from optimized FLB TRF hydrogel compared to the raw FLB gel could be attributed to the drug's improved solubility and permeability by loading on a hydrophobic carrier. Comparing the two intranasal hydrogels, the optimized FLB-TRF-loaded hydrogel shows significant increases in C_{max} and AUC ($p < 0.05$) for both plasma and brain compared to control, indicating higher bioavailability and enhanced brain delivery of the drug. This could be attributed to FLB movement from the nasal cavity along both the olfactory or trigeminal nerves to the parenchyma of the brain. FLB is delivered to the nerves in the cerebrum and pons and then disperses throughout the brain. The intracellular and extracellular pathways are the ways by which FLB brain dispersion occurs. For the intracellular mechanism, FLB is internalized by an olfactory neuron through endocytosis, trafficked within the cell to the neuron's projection site, and then released by exocytosis. For the extracellular pathway, FLB crosses the nasal epithelium to the lamina propria and then is transported externally along the length of the neuronal axon that leads into the CNS, where FLB is distributed by fluid movement. The enhanced drug bioavailability could be ascribed to the improved permeation properties of TRFs owing to their flexible and ultra-deformable structure that enhances penetration across the mucosal barrier [50]. Furthermore, the elevated concentration of the drug in the brain highlights the capability of TRF to augment direct delivery of the drug to the brain through the nasal olfactory region and across the BBB. The nanoscale size of the vesicles might also yield a shielding effect for the drug, protecting it from fast excretion and metabolism and leading to improved CNS delivery [41].

5. Conclusions

TRF-loaded hydrogel has been investigated as a possible intranasal delivery system of FLB. Box–Behnken design was successfully applied for optimization of FLB TRFs with minimized vesicular size. The optimized FLB TRFs (1:1.12 drug:PL molar ratio, surfactant HLB of 2.3, and hydration medium pH of 7.2) were spherical, with a vesicle size of less than 100 nm. The optimized FLB-TRF-loaded hydrogel showed an enhanced ex vivo permeation profile through goat mucosa when compared to that of control FLB hydrogel. In vivo assessment in Wistar rats confirmed that the optimized hydrogel had higher bioavailability than the control and exhibited enhanced brain delivery. Based on these results, the proposed optimized FLB-TRF-loaded hydrogel could be considered a promising drug delivery system for nose-to-brain delivery of the drug.

Author Contributions: Conceptualization, O.A.A.A. and U.A.F.; methodology, S.M.B.-E.; software, H.M.A.; validation, Z.A.A., H.Z.A., and A.K.K.; formal analysis, G.C.; investigation, F.C.; resources, A.A.; data curation, R.A.A.-G. (Raniyah A. Al-Ghamdi); writing—original draft preparation, U.A.F.; writing—review and editing, S.M.B.-E., G.C. and F.C.; visualization, R.A.A.-G. (Rawan A. Al-Ghamdi); supervision, Z.A.A.; project administration, N.A.A.; funding acquisition, N.A.A. All authors have read and agreed to the published version of the manuscript.

References

1. Allers, K.A.; Dremencov, E.; Ceci, A.; Flik, G.; Ferger, B.; Cremers, T.I.F.H.; Ittrich, C.; Sommer, B. Acute and repeated flibanserin administration in female rats modulates monoamines differentially across brain areas: A microdialysis study. *J. Sex. Med.* **2010**, *7*, 1757–1767. [CrossRef] [PubMed]

2. Borsini, F. Method of using flibanserin for neuroprotection. US Patent App. 10/882, 1 July 2004.

3. Kennedy, S. Flibanserin: Initial evidence of efficacy on sexual dysfunction, in patients with major depressive disorder. *J. Sex. Med.* **2010**, *7*, 3449–3459. [CrossRef] [PubMed]

4. Katz, M.; Derogatis, L.R.; Ackerman, R.; Hedges, P.; Lesko, L.; Garcia, M.; Sand, M. Efficacy of flibanserin in women with hypoactive sexual desire disorder: Results from the BEGONIA trial. *J. Sex. Med.* **2013**, *10*, 1807–1815. [CrossRef] [PubMed]

5. Lodise, N.M. Female sexual dysfunction: A focus on flibanserin. *Int. J. Womens Health* **2017**, *9*, 757–767. [CrossRef] [PubMed]

6. Dooley, E.M.; Miller, M.K.; Clayton, A.H. Flibanserin: From Bench to Bedside. *Sex. Med. Rev.* **2017**, *5*, 461–469. [CrossRef]

7. El-Kattan, A.; Varm, M. Oral Absorption, Intestinal Metabolism and Human Oral Bioavailability. In *Topics on Drug Metabolism*; Paxton, J., Ed.; IntechOpen: London, UK, 2012.

8. Erdő, F.; Bors, L.A.; Farkas, D.; Bajza, Á.; Gizurarson, S. Evaluation of intranasal delivery route of drug administration for brain targeting. *Brain Res. Bull.* **2018**, *143*, 155–170. [CrossRef]

9. Lungare, S.; Bowen, J.; Badhan, R. Development and Evaluation of a Novel Intranasal Spray for the Delivery of Amantadine. *J. Pharm. Sci.* **2016**, *105*, 1209–1220. [CrossRef]

10. Cevc, G.; Blume, G. Lipid vesicles penetrate into intact skin owing to the transdermal osmotic gradients and hydration force. *BBA Biomembr.* **1992**, *1104*, 226–232. [CrossRef]

11. Fernández-García, R.; Lalatsa, A.; Statts, L.; Bolás-Fernández, F.; Ballesteros, M.P.; Serrano, D.R. Transferosomes as nanocarriers for drugs across the skin: Quality by design from lab to industrial scale. *Int. J. Pharm.* **2020**, *573*, 118817. [CrossRef] [PubMed]

12. Sarhan, O.; Abdel-Ghany, M.; Abdel-Hamid, M.; Cairo, I. Development, evaluation and application of Transfersomal Green tea extract (Camellia sinensis) formulations. *Am. J. Med. Pharm. Res.* **2020**, *2*, 21–39.

13. Piumitali, B.; Neeraj, U.; Jyotivardhan, J. Transfersomes—A Nanoscience in Transdermal Drug Delivery and Its Clinical Advancements. *Int. J. Nanosci.* **2020**. [CrossRef]

14. Aboud, H.M.; Ali, A.A.; El-Menshawe, S.F.; Elbary, A.A. Nanotransfersomes of carvedilol for intranasal delivery: Formulation, characterization and in vivo evaluation. *Drug Deliv.* **2016**, *23*, 2471–2481.

15. Pitta, S.K.; Dudhipala, N.; Narala, A.; Veerabrahma, K. Development of zolmitriptan transfersomes by Box–Behnken design for nasal delivery: In vitro and in vivo evaluation. *Drug Dev. Ind. Pharm.* **2018**, *44*, 484–492. [CrossRef]

16. Mouez, M.A.; Nasr, M.; Abdel-Mottaleb, M.; Geneidi, A.S.; Mansour, S. Composite chitosan-transfersomal vesicles for improved transnasal permeation and bioavailability of verapamil. *Int. J. Biol. Macromol.* **2016**, *93*, 591–599. [CrossRef] [PubMed]

17. Nasr, M.; Wahdan, S.A. Neuroprotective effects of novel nanosystems simultaneously loaded with vinpocetine and piracetam after intranasal administration. *Life Sci.* **2019**, *226*, 117–129. [CrossRef] [PubMed]

18. Salama, H.A.; Mahmoud, A.A.; Kamel, A.O.; Abdel Hady, M.; Awad, G.A.S. Brain delivery of olanzapine by intranasal administration of transfersomal vesicles. *J. Liposome Res.* **2012**, *22*, 336–345. [CrossRef] [PubMed]

19. Omar, M.M.; Eleraky, N.E.; El Sisi, A.M.; Hasan, O.A. Development and evaluation of in-situ nasal gel formulations of nanosized transferosomal sumatriptan: Design, optimization, in vitro and in vivo evaluation. *Drug Des. Dev. Ther.* **2019**, *13*, 4413–4430. [CrossRef] [PubMed]

20. Shimizu, T.; Kishida, T.; Hasegawa, U.; Ueda, Y.; Imanishi, J.; Yamagishi, H.; Akiyoshi, K.; Otsuji, E.; Mazda, O. Nanogel DDS enables sustained release of IL-12 for tumor immunotherapy. *Biochem. Biophys. Res. Commun.* **2008**, *367*, 330–335. [CrossRef]

21. Sarei, F.; Dounighi, N.; Zolfagharian, H.; Khaki, P.; Bidhendi, S. Alginate nanoparticles as a promising adjuvant and vaccine delivery system. *Indian J. Pharm. Sci.* **2013**, *75*, 442–449.

22. Salatin, S.; Maleki Dizaj, S.; Yari Khosroushahi, A. Effect of the surface modification, size, and shape on cellular uptake of nanoparticles. *Cell Biol. Int.* **2015**, *39*, 881–890. [CrossRef]

23. Salatin, S.; Jelvehgari, M.; Maleki-Dizaj, S.; Adibkia, K. A sight on protein-based nanoparticles as drug/gene delivery systems. *Ther. Deliv.* **2015**, *6*, 1017–1029. [CrossRef]

24. Joysa Ruby, J.; Pandey, V.P. Chitosan nanoparticles as a nasal drug delivery for memantine hydrochloride. *Int. J. Pharm. Pharm. Sci.* **2015**, *7*, 34–37.

25. Salatin, S.; Barar, J.; Barzegar-Jalali, M.; Adibkia, K.; Milani, M.A.; Jelvehgari, M. Hydrogel nanoparticles and nanocomposites for nasal drug/vaccine delivery. *Arch. Pharm. Res.* **2016**, *39*, 1181–1192. [CrossRef] [PubMed]

26. Rigogliuso, S.; Sabatino, M.A.; Adamo, G.; Grimaldi, N.; Dispenza, C.; Ghersi, G. Polymeric nanogels: Nanocarriers for drug delivery application. *Chem. Eng. Trans.* **2012**, *27*, 247–252.

27. Bhavna; Sharma, V.; Ali, M.; Baboota, S.; Ali, J. Preparation and characterization of chitosan nanoparticles for nose to brain delivery of a cholinesterase inhibitor. *Indian J. Pharm. Sci.* **2007**, *69*, 712–713.

28. Gyu Kong, I.; Sato, A.; Yuki, Y.; Nochi, T.; Takahashi, H.; Sawada, S.; Mejima, M.; Kurokawa, S.; Okada, K.; Sato, S.; et al. Nanogel-based pspa intranasal vaccine prevents invasive disease and nasal colonization by streptococcus pneumoniae. *Infect. Immun.* **2013**, *81*, 1625–1634. [CrossRef]

29. Catoira, M.C.; Fusaro, L.; Di Francesco, D.; Ramella, M.; Boccafoschi, F. Overview of natural hydrogels for regenerative medicine applications. *J. Mater. Sci. Mater. Med.* **2019**, *30*, 1–10. [CrossRef]

30. Jerca, F.A.; Anghelache, A.M.; Ghibu, E.; Cecoltan, S.; Stancu, I.C.; Trusca, R.; Vasile, E.; Teodorescu, M.; Vuluga, D.M.; Hoogenboom, R.; et al. Poly(2-isopropenyl-2-oxazoline) Hydrogels for Biomedical Applications. *Chem. Mater.* **2018**, *30*, 7938–7949. [CrossRef]

31. Xu, X.; Jerca, F.A.; Jerca, V.V.; Hoogenboom, R. Covalent Poly(2-Isopropenyl-2-Oxazoline) Hydrogels with Ultrahigh Mechanical Strength and Toughness through Secondary Terpyridine Metal-Coordination Crosslinks. *Adv. Funct. Mater.* **2019**, *29*, 1904886. [CrossRef]

32. Zhao, C.; Lu, X.; Hu, Q.; Liu, S.; Guan, S. PVA/PEG hybrid hydrogels prepared by freeze-thawing and high energy electron beam irradiation. *Chem. Res. Chin. Univ.* **2017**, *33*, 995–999. [CrossRef]

33. Joshi, S.C. Sol-gel behavior of hydroxypropyl methylcellulose (HPMC) in ionic media including drug release. *Materials* **2011**, *4*, 1861–1905. [CrossRef] [PubMed]

34. Pham, A.T.; Lee, P.I. Probing the Mechanisms of Drug Release from Hydroxypropylmethyl Cellulose Matrices. *Pharm. Res. An Off. J. Am. Assoc. Pharm. Sci.* **1994**, *11*, 1379–1384.

35. Zaki, N.M.; Awad, G.A.; Mortada, N.D.; Abd ElHady, S.S. Enhanced bioavailability of metoclopramide HCl by intranasal administration of a mucoadhesive in situ gel with modulated rheological and mucociliary transport properties. *Eur. J. Pharm. Sci.* **2007**, *32*, 296–307. [CrossRef] [PubMed]

36. Escudero, J.J.; Ferrero, C.; Jiménez-Castellanos, M.R. Compaction properties, drug release kinetics and fronts movement studies from matrices combining mixtures of swellable and inert polymers. II. Effect of HPMC with different degrees of methoxy/hydroxypropyl substitution. *Int. J. Pharm.* **2010**, *387*, 56–64. [CrossRef]

37. Colombo, P. Swelling-controlled release in hydrogel matrices for oral route. *Adv. Drug Deliv. Rev.* **1993**, *11*, 37–57. [CrossRef]

38. Badr-Eldin, S.M.S.; Ahmed, O.A.A. Optimized nano-transfersomal films for enhanced sildenafil citrate transdermal delivery: Ex vivo and in vivo evaluation. *Drug Des. Devel. Ther.* **2016**, *10*, 1323–1333. [CrossRef]

39. Galgatte, U.C.; Kumbhar, A.B.; Chaudhari, P.D. Development of in situ gel for nasal delivery: Design, optimization, in vitro and in vivo evaluation. *Drug Deliv.* **2014**, *21*, 62–73. [CrossRef]

40. Ahmed, O.A.A.; Badr-Eldin, S.M. In situ misemgel as a multifunctional dual-absorption platform for nasal delivery of raloxifene hydrochloride: Formulation, characterization, and in vivo performance. *Int. J. Nanomed.* **2018**, *13*, 6325–6335. [CrossRef]

41. Al Asmari, A.K.; Ullah, Z.; Tariq, M.; Fatani, A. Preparation, characterization, and in vivo evaluation of intranasally administered liposomal formulation of donepezil. *Drug Des. Dev. Ther.* **2016**, *10*, 205–215.

42. Young, J. Histopathologic examination of the rat nasal cavity. *Fundam. Appl. Toxicol.* **1981**, *1*, 309–312. [CrossRef]

43. Dubey, V.; Mishra, D.; Dutta, T.; Nahar, M.; Saraf, D.K.; Jain, N.K. Dermal and transdermal delivery of an anti-psoriatic agent via ethanolic liposomes. *J. Control. Release* **2007**, *123*, 148–154. [CrossRef]

44. Abourehab, M.; Ahmed, O.; Balata, G.; Almalki, W. Self-assembled biodegradable polymeric micelles to improve dapoxetine delivery across the blood–brain barrier. *Int. J. Nanomed.* **2018**, *13*, 3679–3687. [CrossRef]

45. El Zaafarany, G.G.M.; Awad, G.G.A.S.; Holayel, S.S.M.; Mortada, N.D.N. Role of edge activators and surface charge in developing ultradeformable vesicles with enhanced skin delivery. *Int. J. Pharm.* **2010**, *397*, 164–172. [CrossRef]

46. El-Laithy, H.M.; Shoukry, O.; Mahran, L.G. Novel sugar esters proniosomes for transdermal delivery of vinpocetine: Preclinical and clinical studies. *Eur. J. Pharm. Biopharm.* **2011**, *77*, 43–55. [CrossRef]

47. Khan, M.I.; Madni, A.; Ahmad, S.; Mahmood, M.A.; Rehman, M.; Ashfaq, M. Formulation design and characterization of a non-ionic surfactant based vesicular system for the sustained delivery of a new chondroprotective agent. *Braz. J. Pharm. Sci.* **2015**, *51*, 607–616. [CrossRef]

48. Ahmed, E.M. Hydrogel: Preparation, characterization, and applications: A review. *J. Adv. Res.* **2015**, *6*, 105–121. [CrossRef]

49. Al-Ghananeem, A.M.; Saeed, H.; Florence, R.; Yokel, R.A.; Malkawi, A.H. Intranasal drug delivery of didanosine-loaded chitosan nanoparticles for brain targeting; An attractive route against infections caused by aids viruses. *J. Drug Target.* **2010**, *18*, 381–388. [CrossRef]

50. Salem, H.F.; Kharshoum, R.M.; Abou-Taleb, H.A.; Naguib, D.M. Nanosized Transferosome-Based Intranasal In Situ Gel for Brain Targeting of Resveratrol: Formulation, Optimization, In Vitro Evaluation, and In Vivo Pharmacokinetic Study. *AAPS PharmSciTech* **2019**, *20*, 181. [CrossRef] [PubMed]